Bioorganic Chemistry 84 (2019) 41–50

Contents lists available at ScienceDirect

Bioorganic Chemistry

journal homepage: www.elsevier.com/locate/bioorg

Synthesis and biological evaluation of new pyrazolone Schiff bases as monoamine oxidase and cholinesterase inhibitors

Fatih Tok[a], Bedia Koçyiğit-Kaymakçıoğlu[a], Begüm Nurpelin Sağlık[b,c], Serkan Levent[b,c], Yusuf Özkay[b,c,*], Zafer Asım Kaplancıklı[b]

[a] Department of Pharmaceutical Chemistry, Faculty of Pharmacy, Marmara University, İstanbul, Turkey
[b] Department of Pharmaceutical Chemistry, Faculty of Pharmacy, Anadolu University, Eskişehir, Turkey
[c] Doping and Narcotic Compounds Analysis Laboratory, Faculty of Pharmacy, Anadolu Universty, Eskişehir, Turkey

ARTICLE INFO

Keywords:
Schiff base
Acetylcholinesterase
Butyrylcholinesterase
Monoamine oxidase A
Monoamine oxidase B
Docking

ABSTRACT

In the current work, Schiff base derivatives of antipyrine were synthesized. The chemical characterization of the compounds was confirmed using IR, ^{1}H NMR, ^{13}C NMR and mass spectroscopies. The inhibitory potency of synthesized compounds was investigated towards acetylcholinesterase (AChE), butyrylcholinesterase (BuChE), and monoamine oxidases A and B (MAO-A and MAO-B) enzymes. Some of the compounds displayed significant inhibitory activity against AChE and MAO-B enzymes, respectively. According to AChE enzyme inhibition assay, compounds **3e** and **3g** were found as the most potent derivatives with IC_{50} values of 0.285 μM and 0.057 μM, respectively. Also, compounds **3a** (IC_{50} = 0.114 μM), **3h** (IC_{50} = 0.049 μM), and **3i** (IC_{50} = 0.054 μM) were the most active derivatives against MAO-B enzyme activity. So as to understand inhibition type, enzyme kinetics studies were carried out. Furthermore, molecular docking studies were performed to define and evaluate the interaction mechanism between compounds **3g** and **3h** and related enzymes. ADME (Absorption, Distribution, Metabolism, and Excretion) and BBB (Blood, Brain, Barier) permeability predictions were applied to estimate pharmacokinetic profiles of synthesized compounds.

1. Introduction

Alzheimer's disease (AD) is a degenerative disease of the central nervous system (CNS), which is characterized by mental deterioration, especially in the elderly. The “cholinergic hypothesis” means the inadequate cholinergic transmission in the synapse and constitutes the basis of treatment in the AD. According to this hypothesis, cholinesterase (ChE) inhibitors increase the acetylcholine level in the synapse and help reverse the symptoms of the disease [1,2]. There are two ChE enzymes. Acetylcholinesterase (AChE) is the main enzyme responsible for acetylcholine (ACh) hydrolysis in the cholinergic synapses, whereas butyrylcholinesterase (BuChE) serves as a co-regulator of AChE activity. While ACh is the substrate of AChE, butyrylcholine (BuCh) is the substrate of BChE and this issue is the main difference between these two enzymes [3,4]. Therapeutic agents which are capable of inhibiting both enzymes may provide additional benefits for AD. Current treatments for AD mainly focus on the use of AChE inhibitors, namely donepezil, rivastigmin, galantamine, which are accepted by the FDA. These drugs have only symptomatic effects, and therefore, there is a need for the discovery of more effective agents to stop the progression of the disease [5–7].

In the regulation of different biological processes, monoamine oxidase (MAO) enzymes play a considerable role and, thereby, they are crucial targets in drug design for the treatment of psychiatric and neurological disorders [8]. MAO-A inhibitors are clinically used predominantly as antidepressant, anxiolytic and against autism [9,10], whereas MAO-B inhibitors are generally used to treat symptoms related to Parkinson's and Alzheimer's disease [11]. Despite their long clinical success, first-generation MAO inhibitors have several problems including interactions with other drugs and tyramine, which is a dietary amine and may cause a fatal hypertensive crisis. In view of these adverse actions and restrictions, the clinical use of first generation of MAO inhibitors have been decreased, whereas second generation MAO inhibitors such as selegiline and moclobemide have come into prominence due to lack of above problems [12,13]. In light of the above-mentioned information, the interest of medical chemists in the development of new and potent MAO inhibitors has increased.

In recent years, investigations on physical, chemical, and biological properties of pyrazoles have given promising information. With their structural multiplicity and degree of nature, the pyrazole derivatives exhibit various pharmacological properties [14]. The change of their

* Corresponding author at: Anadolu University, Faculty of Pharmacy, Department of Pharmaceutical Chemistry, 26470 Eskişehir, Turkey.
E-mail address: yozkay@anadolu.edu.tr (Y. Özkay).

https://doi.org/10.1016/j.bioorg.2018.11.016
Received 13 August 2018; Received in revised form 12 November 2018; Accepted 13 November 2018
Available online 17 November 2018
0045-2068/

structures provides a high degree of diversity, which has proven useful in the investigation of new therapeutic agents. Pyrazole ring system and its hydrogenated analogues pyrazoline and pyrazolidine can be considered as a cyclic hydrazine, which is a pharmacophore in several MAO-inhibitors and also displays high affinity for various enzymes including cholinesterases [15,16]. Thus pyrazole derivatives fit well to design strategy of new effective compounds targeting AChE and/or MAO [17]. In literature there are several studies including enzyme inhibitory activities of pyrazole derivatives against MAO [18–22], AChE [23–25] and both enzymes [26–28].

Above observations encouraged us to perform a study targeting the development of new AChE and/or MAO inhibitors that may be beneficial in the treatment of AD. Thus, herein we present the synthesis and enzyme inhibition studies of new pyrazolone derivatives.

2. Materials and methods

2.1. Chemistry

2.1.1. General

Sigma Aldrich (St. Louis, Mo., USA), S.D Fine Chemicals (India) and Merck (Darmstadt, Germany) are suppliers of chemicals, reagents and solvents used in the study. All solvents and reagents were of reagent grade and used directly without purification. The monitoring of the reaction progress was accomplished by thin layer chromatography (TLC) on commercially available silica gel (Kieselgel 60, F254) coated aluminum layers (Merck) with the solvent system petroleum ether:ethyl acetate (10:90). Electrothermal 9100 digital melting point apparatus (Electrothermal, Essex, UK) and Shimadzu FTIR 8400 S (Kyoto, Japan) were used for melting point and infrared spectroscopy analysis, respectively. Proton and carbon NMR spectra of compounds in DMSO-d_6 were obtained by DPX 300 NMR spectrometry (Bruker Bioscience, Billerica, Mass., USA) and Bruker DPX 75 NMR spectrometry, respectively. The mass measurements were carried out by High Resolution Mass Spectroscopy system Shimadzu LCMS-IT-TOF instrument equipped with SPD-M20A PDA detector (Kyoto, Japan) which was also used to control purity indexes.

2.1.2. Synthesis of 1,5-dimethyl-4-nitroso-2-phenyl-1H-pyrazol-3(2H)-one (1)

Antipyrine (50 mmol, 9.41 g) was dissolved in acetic acid (50 mL). The solution was cooled to 0–5 °C and sodium nitrite (60 mmol, 4.14 g) in water (25 mL). The final solution was stirred for 20 min and then diluted with water. The precipitated product was filtered and dried [29].

2.1.3. Synthesis of 4-amino-1,5-dimethyl-2-phenyl-1H-pyrazol-3(2H)-one (2)

Acetic acid (10 mL) was added on 4-nitrosoantipyrine (23 mmol, 5 g) in water-ethanol solution. The mixture was cooled to 0–5 °C and stirred continuously on a magnetic stirrer. Zinc dust was added in portions until color of the solution changed. The precipitated product was filtered and dried [30].

2.1.4. Synthesis of 4-Substituted antipyrine derivatives (3a-3p)

A mixture of 4-aminoantipyrine (1 mmol, 0.23 g) and appropriate substituted aldehyde (1 mmol) in ethanol (10 mL) was refluxed for 4 h with the presence of a few drops of glacial acetic acid. The reaction was completed by thin layer chromatography control. The precipitate was filtered, dried and purified with methanol [31].

*2.1.4.1. 4-(4-Hydroxybenzylideneamino)-1,5-dimethyl-2-phenyl-1H-pyrazol-3(2H)-one (**3a**).* Yield 72%, m.p. 232 °C. FTIR (ATR, cm^{-1}): 3072 (aromatic C—H), 1654 (C=O), 1579–1425 (C=C, C=N), 1311 (C—O), 1157 (C—N). ^{1}H NMR (300 MHz, DMSO-d_6, ppm) δ 2.41 (s, 3H, C—CH_3), 3.12 (s, 3H, N—CH_3), 6.82–7.66 (m, 9H, Ar—H), 9.46 (s, 1H, =CH—), 9.90 (s, 1H, OH). ^{13}C NMR (75 MHz, DMSO-d_6, ppm) δ 10.26, 36.09, 116.06, 117.51, 124.70, 127.09, 129.30, 129.55, 129.56, 135.23, 152.16, 155.33, 160.13, 160.41 HRMS (*m/z*): $[M+H]^+$ calcd for $C_{18}H_{17}N_3O$: 308.1394; found 308.1396.

*2.1.4.2. 4-(2,4-Dichlorobenzylideneamino)-1,5-dimethyl-2-phenyl-1H-pyrazol-3(2H)-one (**3b**).* Yield 72%, m.p. 211 °C. FTIR (ATR, cm^{-1}): 3049 (aromatic C—H), 2924 (C—H), 1643 (C=O), 1581–1487 (C=C, C=N), 1128 (C—N), 1049 (C—Cl). ^{1}H NMR (300 MHz, DMSO-d_6, ppm) δ 2.48 (s, 3H, C—CH_3), 3.24 (s, 3H, N—CH_3), 7.36–8.18 (m, 8H, Ar—H), 9.92 (s, 1H, =CH—). ^{13}C NMR (75 MHz, DMSO-d_6, ppm) δ 10.14, 35.49, 116.41, 125.51, 127.70, 128.26, 128.32, 129.64, 129.77, 133.95, 134.74, 134.90, 135.37, 148.80, 152.82, 159.65. HRMS (*m/z*): $[M+H]^+$ calcd for $C_{18}H_{15}N_3OCl_2$: 360.0665; found 360.0682.

*2.1.4.3. 1,5-Dimethyl-2-phenyl-4-(4-(piperidin-1-yl)benzylideneamino)-1H-pyrazol-3(2H)-one (**3c**).* Yield 62%, m.p. 217 °C. FTIR (ATR, cm^{-1}): 3052 (aromatic C—H), 2918–2848 (C—H), 1647 (C=O), 1591–1454 (C=C, C=N), 1180 (C—N). ^{1}H NMR (300 MHz, DMSO-d_6, ppm) δ 1.58 (s, 6H, piperidine —CH_2—), 2.41 (s, 3H, C—CH_3), 3.11 (s, 3H, N—CH_3), 3.32 (s, 4H, piperidine N—CH_2—), 6.94–7.64 (m, 9H, Ar—H), 9.45 (s, 1H, =CH—). ^{13}C NMR (75 MHz, DMSO-d_6, ppm) δ 10.28, 24.41, 25.45, 36.19, 48.92, 114.95, 117.89, 124.59, 127.00, 127.46, 129.11, 129.53, 135.30, 151.95, 153.07, 155.51, 160.53. HRMS (*m/z*): $[M+H]^+$ calcd for $C_{23}H_{26}N_4O$: 375.2179; found 375.2182.

*2.1.4.4. 4-(3-Ethoxy-4-hydroxybenzylideneamino)-1,5-dimethyl-2-phenyl-1H-pyrazol-3(2H)-one (**3d**).* Yield 72%, m.p. 218 °C. FTIR (ATR, cm^{-1}): 3115 (aromatic C—H), 2972–2918 (C—H), 1620 (C=O), 1575–1415 (C=C, C=N), 1375 (C—O), 1126 (C—N). ^{1}H NMR (300 MHz, DMSO-d_6, ppm) δ 1.34 (t, 3H, CH_3), 2.43 (s, 3H, C—CH_3), 3.13 (s, 3H, N—CH_3), 4.05 (q, 2H, —OCH_2—), 6.84–7.55 (m, 8H, Ar—H), 9.42 (s, 1H, =CH–). ^{13}C NMR (75 MHz, DMSO-d_6, ppm) δ 10.30, 15.20, 36.10, 64.27, 111.31, 115.97, 124.70, 127.09, 129.30, 129.55, 129.56, 135.23, 152.16, 155.33, 160.13, 160.41. HRMS (*m/z*): $[M+H]^+$ calcd for $C_{20}H_{21}N_3O_3$: 352.1656; found 352.1662.

*2.1.4.5. 4-(2,6-Dimethylbenzylideneamino)-1,5-dimethyl-2-phenyl-1H-pyrazol-3(2H)-one (**3e**).* Yield 65%, m.p. 119 °C. FTIR (ATR, cm^{-1}): 3062 (aromatic C—H), 2914 (C—H), 1651 (C=O), 1593–1402 (C=C, C=N), 1134 (C—N). ^{1}H NMR (300 MHz, DMSO-d_6, ppm) δ 2.41 (s, 3H, C—CH_3), 2.48 (s, 6H, Ar—CH_3), 3.17 (s, 3H, N—CH_3), 7.07–7.55 (m, 8H, Ar—H), 9.94 (s, 1H, =CH—). ^{13}C NMR (75 MHz, DMSO-d_6, ppm) δ 10.26, 21.52, 35.84, 117.72, 124.99, 127.28, 129.10, 129.33, 129.56, 134.44, 135.05, 137.82, 152.69, 156.38, 159.97. HRMS (*m/z*): $[M+H]^+$ calcd for $C_{20}H_{21}N_3O$: 320.1757; found 320.1764.

*2.1.4.6. 4-(2,6-Dichlorobenzylideneamino)-1,5-dimethyl-2-phenyl-1H-pyrazol-3(2H)-one (**3f**).* Yield 72%, m.p. 199 °C. FTIR (ATR, cm^{-1}): 3047 (aromatic C—H), 2929 (C—H), 1647 (C=O), 1579–1413 (C=C, C=N), 1307 (C—O), 1192 (C—N), 1087 (C—Cl). ^{1}H NMR (300 MHz, DMSO-d_6, ppm) δ 2.42 (s, 3H, C—CH_3), 3.23 (s, 3H, N—CH_3), 7.37–7.56 (m, 8H, Ar—H), 9.77 (s, 1H, =CH—). ^{13}C NMR (75 MHz, DMSO-d_6, ppm) δ 10.12, 35.42, 116.06, 125.58, 127.72, 129.64, 129.83, 131.14, 133.38, 134.29, 134.71, 150.19, 153.03, 159.46. HRMS (*m/z*): $[M+H]^+$ calcd for $C_{18}H_{15}N_3OCl_2$: 360.0665; found 360.0680.

*2.1.4.7. 4-(4-(3-(Dimethylamino)propoxy)benzylideneamino)-1,5-dimethyl-2-phenyl-1H-pyrazol-3(2H)-one (**3g**).* Yield 79%, m.p. 146 °C. FTIR (ATR, cm^{-1}): 3072 (aromatic C—H), 2924–2802 (C—H), 1647 (C=O), 1606–1423 (C=C, C=N), 1311 (C—O), 1157 (C—N). ^{1}H NMR (300 MHz, DMSO-d_6, ppm) δ 1.80 (m, 2H, CH_2), 2.13 (s, 6H, N—CH_3), 2.31 (t, 2H, NCH_2), 2.42 (s, 3H, C—CH_3), 3.13 (s, 3H, N—CH_3), 4.01 (t, 2H, OCH_2), 6.97–7.75 (m, 9H, Ar—H), 9.51 (s, 1H, =CH—). ^{13}C NMR (75 MHz, DMSO-d_6, ppm) δ 10.23, 27.31, 35.99, 45.66, 56.08, 66.42, 115.10, 117.25, 124.80, 127.18, 129.35, 129.58, 130.66, 135.13,

152.31, 154.81, 160.29, 160.92. HRMS (*m/z*): $[M+H]^+$ calcd for $C_{23}H_{28}N_4O$: 393.2285; found 393.2286.

*2.1.4.8. 1,5-Dimethyl-4-(4-nitrobenzylideneamino)-2-phenyl-1H-pyrazol-3(2H)-one (**3h**)*. Yield 72%, m.p. 259 °C. FTIR (ATR, cm^{-1}): 3078 (aromatic C−H), 2960 (C−H), 1637 (C═O), 1570–1487 (C═C, C═N, NO_2), 1128 (C−N). ^{1}H NMR (300 MHz, DMSO-d_6, ppm) δ 2.48 (s, 3H, C−CH_3), 3.25 (s, 3H, N−CH_3), 7.36–8.30 (m, 9H, Ar−H), 9.66 (s, 1H, ═CH−). ^{13}C NMR (75 MHz, DMSO-d_6, ppm) δ 10.16, 35.42, 124.48, 125.74, 127.86, 128.37, 129.70, 134.70, 144.05, 148.24, 151.27, 152.85, 159.45, 164.07. HRMS (*m/z*): $[M+H]^+$ calcd for $C_{18}H_{16}N_4O_3$: 337.1295; found 337.1308.

*2.1.4.9. 1,5-Dimethyl-4-(3-nitrobenzylideneamino)-2-phenyl-1H-pyrazol-3(2H)-one (**3i**)*. Yield 72%, m.p. 218 °C. FTIR (ATR, cm^{-1}): 3061 (aromatic C−H), 2945–2877 (C−H), 1620 (C═O), 1593–1413 (C═C, C═N, NO_2), 1136 (C−N). ^{1}H NMR (300 MHz, DMSO-d_6, ppm) δ 2.48 (s, 3H, C−CH_3), 3.22 (s, 3H, N−CH_3), 7.36–8.58 (m, 9H, Ar−H), 9.65 (s, 1H, ═CH−). ^{13}C NMR (75 MHz, DMSO-d_6, ppm) δ 10.21, 35.51, 115.94, 121.00, 124.62, 125.49, 127.70, 129.68, 130.84, 134.09, 134.74, 139.74, 148.80, 151.65, 152.73, 159.62. HRMS (*m/z*): $[M+H]^+$ calcd for $C_{18}H_{16}N_4O_3$: 337.1295; found 337.1310.

*2.1.4.10. 4-(4-Chlorobenzylideneamino)-1,5-dimethyl-2-phenyl-1H-pyrazol-3(2H)-one (**3j**)*. Yield 72%, m.p. 254 °C. FTIR (ATR, cm^{-1}): 3059 (aromatic C−H), 2941 (C−H), 1647 (C═O), 1591–1481 (C═C, C═N), 1132 (C−N), 1070 (C−Cl). ^{1}H NMR (300 MHz, DMSO-d_6, ppm) δ 2.45 (s, 3H, C−CH_3), 3.19 (s, 3H, N−CH_3), 7.35–7.84 (m, 9H, Ar−H), 9.56 (s, 1H, ═CH−). ^{13}C NMR (75 MHz, DMSO-d_6, ppm) δ 10.19, 35.71, 116.46, 125.22, 127.49, 129.24, 129.29, 129.63, 134.98, 136.90, 152.68, 153.13, 159.93. HRMS (*m/z*): $[M+H]^+$ calcd for $C_{18}H_{16}N_3OCl$: 326.1055; found 326.1061.

*2.1.4.11. 4-(3,4-Dichlorobenzylideneamino)-1,5-dimethyl-2-phenyl-1H-pyrazol-3(2H)-one (**3k**)*. Yield 72%, m.p. 239 °C. FTIR (ATR, cm^{-1}): 3084 (aromatic C−H), 2964 (C−H), 1643 (C═O), 1589–1411 (C═C, C═N), 1132 (C−N), 1022 (C−Cl). ^{1}H NMR (300 MHz, DMSO-d_6, ppm) δ 2.47 (s, 3H, C−CH_3), 3.21 (s, 3H, N−CH_3), 7.35–8.04 (m, 8H, Ar-H), 9.52 (s, 1H, ═CH−). ^{13}C NMR (75 MHz, DMSO-d_6, ppm) δ 10.19, 35.57, 116.10, 125.40, 127.64, 128.66, 129.65, 129.66, 131.45, 132.22, 132.59, 134.84, 138.79, 151.42, 152.77, 159.71. HRMS (*m/z*): $[M+H]^+$ calcd for $C_{18}H_{15}N_3OCl_2$: 360.0665; found 360.0672.

*2.1.4.12. 4-(2-Hydroxybenzylideneamino)-1,5-dimethyl-2-phenyl-1H-pyrazol-3(2H)-one (**3l**)*. Yield 72%, m.p. 202 °C. FTIR (ATR, cm^{-1}): 3064 (aromatic C−H), 2937 (C−H), 1651 (C═O), 1589–1411 (C═C, C═N), 1303 (C−O), 1199 (C−N). ^{1}H NMR (300 MHz, DMSO-d_6, ppm) δ 2.40 (s, 3H, C−CH_3), 3.20 (s, 3H, N−CH_3), 6.89–7.57 (m, 9H, Ar−H), 9.70 (s, 1H, ═CH−), 12.94 (s, 1H, OH). ^{13}C NMR (75 MHz, DMSO-d_6, ppm) δ 10.31, 35.61, 114.52, 116.86, 119.64, 120.68, 125.43, 127.72, 129.68, 131.54, 132.20, 134.69, 150.67, 157.97, 159.58, 159.90. HRMS (*m/z*): $[M+H]^+$ calcd for $C_{18}H_{17}N_3O_2$: 308.1394; found 308.1404.

*2.1.4.13. 4-(4-(4-Chlorophenoxy)benzylideneamino)-1,5-dimethyl-2-phenyl-1H-pyrazol-3(2H)-one (**3m**)*. Yield 72%, m.p. 134 °C. FTIR (ATR, cm^{-1}): 3061 (aromatic C−H), 2962 (C−H), 1641 (C═O), 1571–1438 (C═C, C═N), 1305 (C−O), 1130 (C−N), 1008 (C−Cl). ^{1}H NMR (300 MHz, DMSO-d_6, ppm) δ 2.41 (s, 3H, C−CH_3), 3.18 (s, 3H, N−CH_3), 7.06–7.58 (m, 13H, Ar−H), 9.54 (s, 1H, ═CH−). ^{13}C NMR (75 MHz, DMSO-d_6, ppm) δ 10.17, 35.71, 116.68, 120.89, 123.76, 125.18, 127.46, 127.86, 129.62, 130.41, 131.03, 134.96, 140.25, 152.69, 153.65, 155.95, 157.23, 159.91. HRMS (*m/z*): $[M+H]^+$ calcd for $C_{24}H_{20}N_3O_2Cl$: 418.1317; found 418.1324.

*2.1.4.14. Methyl 4-((1,5-dimethyl-3-oxo-2-phenyl-2,3-dihydro-1H-pyrazol-4-ylimino)methyl)benzoate (**3n**)*. Yield 72%, m.p. 207 °C. FTIR (ATR, cm^{-1}): 3042 (aromatic C−H), 2989–2953 (C−H), 1708 (C═O ester), 1647 (C═O), 1556–1408 (C═C, C═N), 1305 (C−O), 1190 (C−N). ^{1}H NMR (300 MHz, DMSO-d_6, ppm) δ 2.41 (s, 3H, C−CH_3), 3.22 (s, 3H, N−CH_3), 3.87 (s, 3H, O−CH_3), 7.36–8.03 (m, 9H, Ar−H), 9.63 (s, 1H, ═CH−). ^{13}C NMR (75 MHz, DMSO-d_6, ppm) δ 10.19, 35.57, 52.67, 116.34, 125.45, 127.65, 127.69, 129.66, 130.04, 130.82, 134.84, 142.27, 152.80, 152.87, 159.72, 166.40. HRMS (*m/z*): $[M+H]^+$ calcd for $C_{20}H_{19}N_3O_3$: 350.1499; found 350.1498.

*2.1.4.15. 4-(4-(benzyloxy)benzylideneamino)-1,5-dimethyl-2-phenyl-1H-pyrazol-3(2H)-one (**3o**)*. Yield 72%, m.p. 188 °C. FTIR (ATR, cm^{-1}): 3047 (aromatic C−H), 2943–2879 (C−H), 1633 (C═O), 1600–1413 (C═C, C═N), 1301 (C−O), 1130 (C−N). ^{1}H NMR (300 MHz, DMSO-d_6, ppm) δ 2.42 (s, 3H, C−CH_3), 3.14 (s, 3H, N−CH_3), 5.16 (s, 2H, O−CH_2), 7.07–7.77 (m, 14H, Ar−H), 9.51 (s, 1H, ═CH−). ^{13}C NMR (75 MHz, DMSO-d_6, ppm) δ 10.25, 35.97, 69.81, 115.50, 117.19, 124.84, 127.21, 128.25, 128.40, 128.94, 129.34, 129.59, 130.98, 135.12, 137.24, 152.35, 154.68, 160.26, 160.57. HRMS (*m/z*): $[M+H]^+$ calcd for $C_{25}H_{23}N_3O_2$: 398.1863; found 398.1868.

*2.1.4.16. 4-(Benzylideneamino)-1,5-dimethyl-2-phenyl-1H-pyrazol-3(2H)-one (**3p**)*. Yield 72%, m.p. 179 °C. FTIR (ATR, cm^{-1}): 3045 (aromatic C−H), 2945 (C−H), 1647 (C═O), 1595–1415 (C═C, C═N), 1303 (C−O), 1157 (C−N). ^{1}H NMR (300 MHz, DMSO-d_6, ppm) δ 2.45 (s, 3H, C−CH_3), 3.17 (s, 3H, N−CH_3), 7.35–7.82 (m, 10*H*, Ar-H), 9.59 (s, 1H, ═CH). ^{13}C NMR (75 MHz, DMSO-d_6, ppm) δ 10.21, 35.78, 116.73, 125.08, 127.38, 127.68, 129.20, 129.62, 130.63, 134.99, 137.97, 152.66, 154.79, 160.05. HRMS (*m/z*): $[M+H]^+$ calcd for $C_{18}H_{17}N_3O$: 292.1444; found 292.1448.

2.2. Biological evaluation

2.2.1. Cholinesterase inhibition assay

AChE and BChE inhibitory activity of all synthesized compounds were evaluated by modified Ellman's spectrophotometric method [32]. All chemicals, reagents and reference drugs (AChE (E.C.3.1.1.7, from electric eel), BChE (from equine serum), 5,5′-dithiobis-(2-nitrobenzoic acide) (DTNB), acetylthiocholine iodide (ATC), butyrylthiocholine iodide (BTC), donepezil hydrochloride and tacrine) used in the method were supplied from Sigma-Aldrich (Germany) and Fluka (Germany). AChE and BChE enzyme inhibition assay were applied as previously described [3,33].

2.2.2. AChE kinetics assay

AChE enzyme kinetics study was performed for compound **3g** to determine the inhibition type. The compound was prepared at three different concentrations (IC_{50}, 2xIC_{50} and IC_{50}/2). The substrate (ATC) was used at various concentrations (600, 300, 150, 75, 37.5 and 18.75 μM). The enzyme kinetics assay was carried out as in our previous publications [3,33]. Lineweaver-Burk plots were formed by using Microsoft Office Excel 2013. The K_i values of the compound were easily calculated from second plot with a common intercept on the x-axis (corresponding to $-K_i$).

2.2.3. MAO inhibition assay

MAO inhibition assay including fluorometric measurement of Ampliflu™ Red (10-Acetyl-3,7-dihydroxyphenoxazine) was performed. Inhibitory activity of synthesized compounds (**3a–3p**) against MAO-A and MAO-B enzymes was measured as reported earlier [12,13,34].

2.2.4. MAO kinetics assay

MAO enzyme kinetics assay was carried out with the same materials used in the MAO inhibitory activity. Tyramine was used as a substrate at the following concentrations: 20, 10, 5, 2.5, 1.25, and 0.625 μM. In order to specify the inhibition type on MAO-B enzyme, compound **3h**

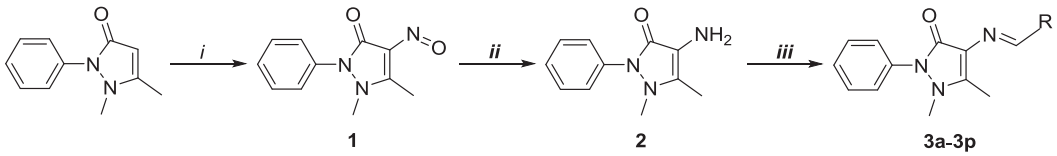

i: $NaNO_2$, CH_3COOH; *ii*: CH_3COOH, Zn, C_2H_5OH; *iii*: Substituted aldehyde, CH_3COOH, C_2H_5OH

*	R	*	R
3a	4-hidroxyphenyl	**3i**	3-nitrophenyl
3b	2,4-dichlorophenyl	**3j**	4-chlorophenyl
3c	4-(piperidino)phenyl	**3k**	3,4-dichlorophenyl
3d	3-ethoxy-4-hidroxyphenyl	**3l**	2-hidroxyphenyl
3e	2,6-dimethylphenyl	**3m**	4-[4-(chlorophenoxy)]phenyl
3f	2,6-dichlorophenyl	**3n**	4-(methoxycarbonyl)phenyl
3g	4-[3-(dimethylamino)propoxy]phenyl	**3o**	4-(benzyloxy)phenyl
3h	4-nitrophenyl	**3p**	phenyl

Scheme 1. The synthetic route of the compounds (**3a–3p**).

Table 1
% Inhibition of the synthesized compounds **3a–3p** and reference agents against AChE, BChE, MAO-A and MAO-B enzymes at concentrations of 10^{-3} and 10^{-4} M.

Comp.	AChE inhibition %		BChE inhibition %		MAO-A inhibition %		MAO-B inhibition %	
	10^{-3} M	10^{-4} M	10^{-3} M	10^{-4} M	10^{-3} M	10^{-4} M	10^{-3} M	10^{-4} M
3a	30.88 ± 0.58	16.28 ± 0.41	30.88 ± 0.58	16.28 ± 0.41	55.28 ± 0.75	25.11 ± 0.60	94.27 ± 1.25	85.13 ± 1.08
3b	28.15 ± 0.61	14.10 ± 0.50	28.15 ± 0.61	14.10 ± 0.50	44.13 ± 0.62	20.48 ± 0.50	68.25 ± 1.05	39.30 ± 0.97
3c	85.26 ± 1.56	78.20 ± 1.20	85.26 ± 1.56	78.20 ± 1.20	58.21 ± 0.74	30.22 ± 0.48	62.19 ± 1.08	34.75 ± 0.88
3d	44.71 ± 0.94	25.99 ± 0.74	44.71 ± 0.94	25.99 ± 0.74	51.03 ± 0.43	24.77 ± 0.40	75.29 ± 0.96	40.17 ± 0.71
3e	21.30 ± 0.63	14.79 ± 0.47	21.30 ± 0.63	14.79 ± 0.47	48.23 ± 0.58	22.42 ± 0.37	68.26 ± 1.00	42.49 ± 0.84
3f	40.79 ± 0.48	28.39 ± 0.41	40.79 ± 0.48	28.39 ± 0.41	33.18 ± 0.66	27.88 ± 0.40	65.29 ± 0.87	44.30 ± 0.52
3g	96.28 ± 1.36	88.12 ± 1.07	96.28 ± 1.36	88.12 ± 1.07	42.27 ± 0.59	19.39 ± 0.41	52.28 ± 0.63	34.36 ± 0.51
3h	35.29 ± 0.63	30.20 ± 0.52	35.29 ± 0.63	30.20 ± 0.52	38.17 ± 0.52	18.26 ± 0.30	98.20 ± 1.19	89.10 ± 1.24
3i	37.18 ± 0.55	31.66 ± 0.40	37.18 ± 0.55	31.66 ± 0.40	42.16 ± 0.58	28.51 ± 0.41	93.28 ± 1.29	87.22 ± 1.18
3j	25.08 ± 0.75	20.60 ± 0.69	25.08 ± 0.75	20.60 ± 0.69	49.33 ± 0.63	30.08 ± 0.47	70.29 ± 0.95	42.46 ± 0.81
3k	36.79 ± 0.67	31.22 ± 0.54	36.79 ± 0.67	31.22 ± 0.54	51.80 ± 0.44	38.15 ± 0.31	66.24 ± 0.63	45.29 ± 0.48
3l	43.81 ± 0.76	24.08 ± 0.81	43.81 ± 0.76	24.08 ± 0.81	42.29 ± 0.67	21.74 ± 0.42	52.46 ± 0.38	34.19 ± 0.27
3m	31.12 ± 0.85	19.25 ± 0.70	31.12 ± 0.85	19.25 ± 0.70	39.26 ± 0.43	18.14 ± 0.33	53.28 ± 0.62	45.49 ± 0.54
3n	50.49 ± 1.25	31.23 ± 0.73	50.49 ± 1.25	31.23 ± 0.73	46.34 ± 0.56	40.77 ± 0.27	61.29 ± 0.75	40.29 ± 0.62
3o	30.28 ± 0.82	24.67 ± 0.76	30.28 ± 0.82	24.67 ± 0.76	48.26 ± 0.55	27.54 ± 0.31	54.16 ± 0.75	35.19 ± 0.52
3p	49.16 ± 0.89	40.28 ± 0.82	49.16 ± 0.89	40.28 ± 0.82	35.61 ± 0.41	24.62 ± 0.30	58.22 ± 0.55	28.16 ± 0.39
Ref-1	99.48 ± 1.92	98.56 ± 1.76	–	–	–	–	–	–
Ref-2	–	–	94.12 ± 2.76	82.14 ± 2.69	–	–	–	–
Ref-3	–	–	–	–	98.91 ± 1.28	96.88 ± 1.31	–	–
Ref-4	–	–	–	–	–	–	98.91 ± 1.28	96.88 ± 1.31

Ref-1: Donepezil, **Ref-2**: Tacrine, **Ref-3**: Moclobemide, **Ref-4**: Selegiline.

Table 2
Evaluation of **3c**, **3g** and donepezil against AChE at further concentrations and IC_{50} values.

Compound	10^{-5} M	10^{-6} M	10^{-7} M	10^{-8} M	10^{-9} M	IC_{50} (μM)
3c	65.79 ± 1.13	58.97 ± 0.98	46.77 ± 0.85	35.60 ± 0.76	20.08 ± 0.54	0.285 ± 0.009
3g	85.17 ± 1.28	77.39 ± 1.02	63.44 ± 1.18	40.89 ± 0.94	21.63 ± 0.52	0.057 ± 0.002
Donepezil	95.30 ± 1.64	92.15 ± 1.88	81.36 ± 1.41	41.78 ± 0.84	25.62 ± 0.58	0.029 ± 0.001

was prepared at the concentrations of $IC_{50}/2$, IC_{50} and $2 \times IC_{50}$. Enzyme kinetics assay was applied according to previous publications [12,13,34].

2.2.5. Prediction of ADME parameters and BBB permeability

QikProp 4.8 software [35] was used to calculate ADME parameters and BBB permeability of all final compounds (**3a–3p**).

2.2.6. Molecular docking studies

Molecular docking studies were performed to discover the binding modes of compounds **3g** and **3h** to active sites of AChE and MAO-B enzymes, respectively. The crystal structures of AChE (PDB code: 4EY7) [36] and MAO-B (PDB code: 2V5Z) [37] were retrieved from the Protein Data Bank server (www.pdb.org). Docking procedures were followed as reported previously [3,12,13,34].

Table 3
IC_{50} values of **3a**, **3h**, **3i** and selegiline against MAO-B.

Compound	10^{-5} M	10^{-6} M	10^{-7} M	10^{-8} M	10^{-9} M	IC_{50} (μM)
3a	74.29 ± 1.11	67.19 ± 0.87	54.22 ± 0.76	34.75 ± 0.79	20.30 ± 0.54	0.114 ± 0.003
3 h	81.00 ± 1.05	76.46 ± 1.14	67.19 ± 0.97	40.29 ± 0.82	25.74 ± 0.76	0.049 ± 0.002
3i	79.17 ± 1.06	72.63 ± 0.97	62.29 ± 0.84	39.97 ± 0.76	22.11 ± 0.62	0.054 ± 0.002
Selegiline	86.96 ± 1.82	79.23 ± 1.72	65.37 ± 1.13	43.28 ± 1.03	14.70 ± 0.26	0.040 ± 0.002

3. Results and discussion

3.1. Chemistry

The synthesis scheme of the target compounds (**3a–3p**) is outlined in Scheme 1. Schiff base derivatives were prepared by reacting various aldehydes and 4-aminoantipyrine. Structure determination and biological evaluation of the final compounds have been made firstly in this study. The structures of synthesized compounds (**3a–3p**) were confirmed by IR, ^{1}H NMR, ^{13}C NMR and mass spectroscopy. IR spectra of the compounds afforded C—H stretching bands of aromatic rings (3115–3030 cm^{-1}) and C=O stretching bands of hydrazide moiety (1681–1620 bands. In the ^{1}H NMR spectra, C—H proton of Schiff base derivatives resonated as a singlet peak at 9.94–9.42 ppm. Methyl groups attached to 1st and 5th positions of pyrazolone ring were observed at 3.11–3.25 ppm and 2.40–2.48 ppm as two singlets, respectively. The protons on the aromatic ring were recorded between 6.82 and 8.58 ppm. The other aliphatic groups were observed at the expected shifting values. In the ^{13}C NMR spectra, methyl carbons on the pyrazolone ring had peaks at 10 and 36 ppm. The signal due to the hydrazide carbonyl carbons appeared at 169.15–159.46 ppm. The signal due to the Schiff base carbons were observed at 162.32–152.73 ppm. Other aromatic carbons were recorded between 111 ppm and 158 ppm. The results of the MS analysis agreed well with the calculated mass of the compounds. The purity of all compounds was controlled by a PDA detector and found to be greater than 97%.

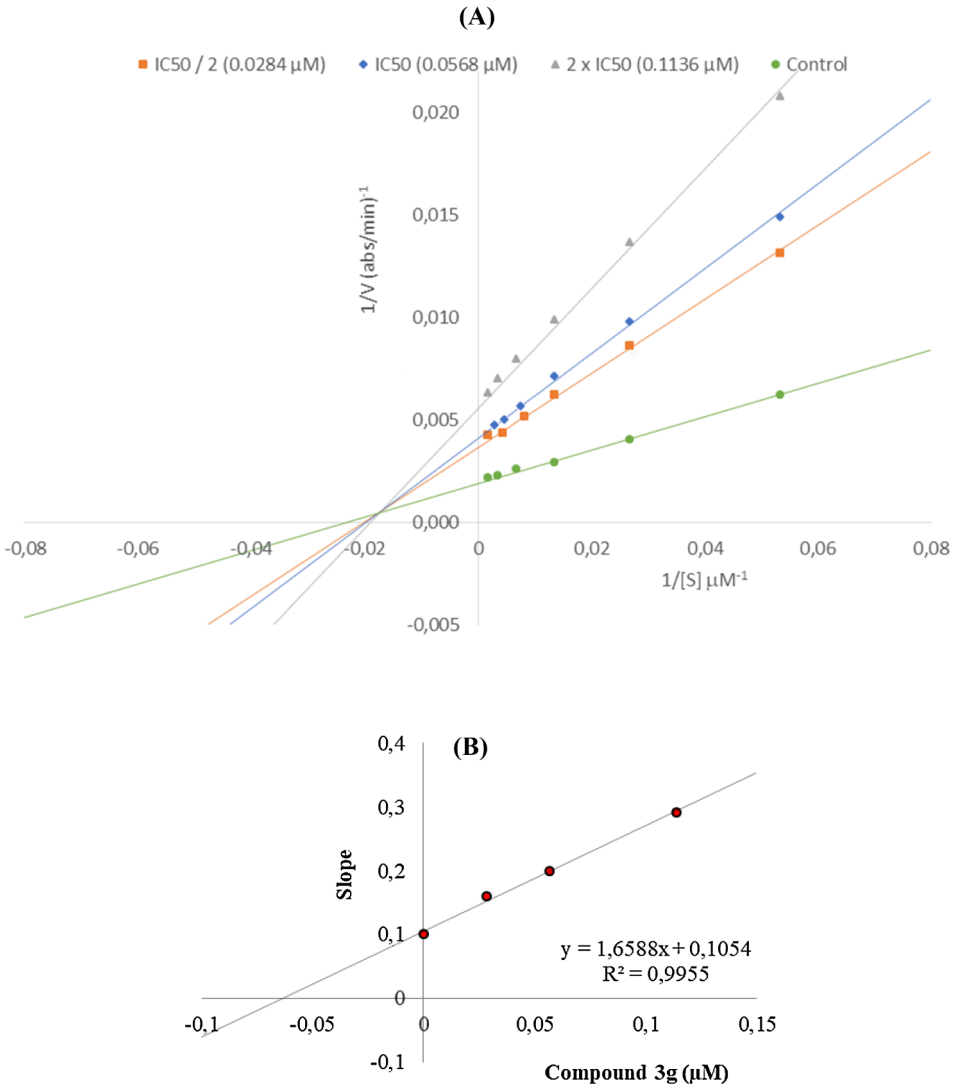

Fig. 1. (A) Lineweaver–Burk plots for the inhibition of AChE by compound **3g**. [S], substrate concentration (μM); V, reaction velocity (abs/min)-1. Vmax values from 2 × IC_{50} to Control; 178.571, 243.902, 270.275 and 434.738 $(abs/min)^{-1}$. Km values of the mixed type inhibition; 52.179, 48.537, 43.243, 50.348 (μM). (B) Secondary plot for calculation of steady-state inhibition constant (K_i) of compound **3g**. Ki was calculated as 0.0635 μM.

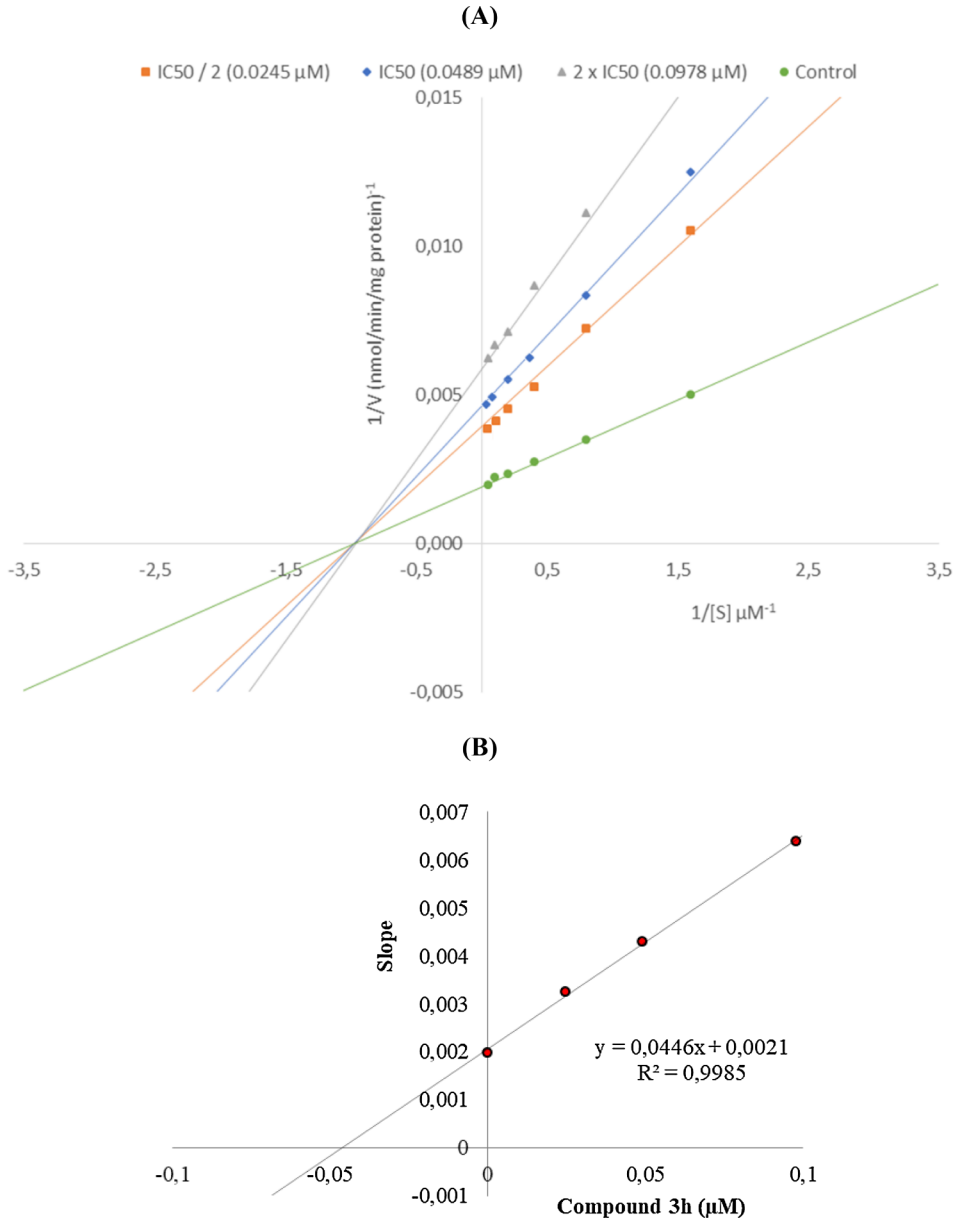

Fig. 2. (A) Lineweaver–Burk plots for the inhibition of MAO-B by compound **3h**. [S], substrate concentration (µM); V, reaction velocity (nmol/min/mg protein). Inhibitor concentrations are shown at the left. V_{max} values from 2 × IC_{50} to Control; 169.492, 212.766, 250.000 and 526.316 (nmol/min/mg protein). K_m value of the non-competitive inhibition; 0.966 ± 0.029 (µM). (B) Secondary plot for calculation of steady-state inhibition constant (K_i) of compound **3h**. K_i was calculated as 0.0471 µM.

3.2. Biological evaluation

3.2.1. Enzyme inhibition

Synthesized compounds were evaluated for their anticholinesterase and MAO inhibitory activities by using in vitro spectrophotometric and fluorimetric methods, respectively [3,12,13,21,34]. Both assays were carried out in two steps. Firstly, compounds **3a–3p** were tested at 10^{-3} and 10^{-4} M concentrations. Selected compounds that indicate promising inhibitory activity at initial concentrations were taken into second step at concentrations of 10^{-5} to 10^{-9} M.

Table 1 displays the anticholinesterase and MAO inhibitory activities of compounds **3a–3p** at 10^{-3} and 10^{-4} M concentrations. None of the compounds displayed noteworthy activity against BChE enzyme. MAO-A inhibition potency of the compounds was almost at low levels. Although most of the compounds were not able to inhibit AChE, compounds **3c** and **3g** differed from the series with their intrinsic inhibitory potential against AChE. Thus, these compounds were diluted and tested in further concentrations (10^{-5} to 10^{-9} M) against AChE along with a reference drug donepezil (Table 2). The IC_{50} values on AChE were recorded as 0.285 µM, 0.057 µM and 0.029 µM for **3c**, **3g** and donepezil, respectively. MAO-B were the most sensitive enzyme against the synthesized compounds. All compounds indicated more than 50% inhibition potency at a concentration of 10^{-3} M. Furthermore, compounds **3a**, **3h** and **3i** showed significant inhibition and thus they were assessed in the second step test. IC_{50} values of compounds **3a**, **3h**, **3i** and selegiline against MAO-B were calculated as 0.114 µM, 0.049 µM, 0.054 µM and 0.040 µM, respectively (Table 3).

Results of enzyme inhibition studies revealed that substituent variation strongly affects the inhibition potency of compounds. Basic nitrogen atom in the substituents of **3c** and **3g** caused a significant increase in AChE activity. On the other hand, incorporation of a strong electron withdrawing nitro group enhanced the MAO-B activity of **3h** and **3i**.

Table 4
Calculated ADME parameters of compounds (**3a–3p**).

Comp	MW	RB	DM	MV	DHB	AHB	PSA	logP	logS	PCaco	logBB	PM	PMDCK	CNSAS	%HOA	VRF	VRT
3a	307.351	4	5.865	1026.605	1	5.75	64.044	2.819	−3.985	1164.223	−0.641	2	583.079	0	100	0	0
3b	360.242	3	8.498	1140.063	0	5	41.380	4.913	−6.142	4422.829	0.313	1	10000.000	1	100	0	1
3c	374.485	3	6.642	1277.142	0	6	46.600	4.788	−6.303	3783.479	−0.092	1	2084.405	0	100	0	1
3d	351.404	6	7.123	1168.814	1	6.5	71.339	3.591	−5.236	1242.236	−0.809	3	625.423	-1	100	0	0
3e	319.405	3	6.666	1136.613	0	5	36.774	4.467	−5.188	5254.316	0.099	3	2972.643	1	100	0	0
3f	360.242	3	5.144	1150.378	0	5	38.214	4.923	−6.467	4723.673	0.258	1	9475.216	1	100	0	1
3g	392.500	8	4.615	1342.549	0	7.75	53.453	3.846	−4.056	924.503	−0.022	3	502.783	1	100	0	0
3h	336.349	4	16.148	1085.835	0	6	90.028	2.800	−4.081	397.230	−1.167	2	182.374	-2	89.857	0	0
3i	336.349	4	11.784	1085.835	0	6	90.028	2.800	−4.081	397.230	−1.167	2	182.374	-2	89.857	0	0
3j	325.797	3	8.493	1047.548	0	5	41.364	4.093	-4.958	3864.616	0.13	1	5261.801	1	100	0	0
3k	360.242	3	9.083	1087.846	0	5	41.362	4.534	−5.597	3864.021	0.266	1	10000.000	1	100	0	0
3l	307.351	4	4.415	1022.291	1	5.75	62.229	2.836	−3.975	1638.697	−0.479	2	843.719	0	100	0	0
3m	417.894	5	8.503	1298.972	0	5.5	49.458	5.634	−6.696	3864.925	−0.026	1	5262.255	0	100	1	1
3n	349.388	4	9.592	1155.973	0	7	76.315	3.169	−4.556	1217.414	−0.684	1	611.926	0	100	0	0
3o	397.476	6	6.874	1327.105	0	5.75	49.251	5.507	−6.586	3864.891	−0.282	3	2132.927	0	100	1	1
3p	291.352	3	6.259	1003.435	0	5	41.361	3.588	−4.191	3864.891	−0.035	1	2132.926	0	100	0	0

MW: Molecular weight, **RB:** Number of rotatable bonds, **DM:** Computed dipole moment, **MV:** Total solvent-accessible volume, **DHB:** Estimated number of hydrogen bond donors, **AHB:** Estimated number of hydrogen bond acceptors, **PSA:** Van der Waals surface area of polar nitrogen and oxygen atoms and carbonyl carbon atoms, **logP:** Predicted octanol/water partition coefficient, **logS:** Predicted aqueous solubility, **PCaco:** Predicted apparent Caco-2 cell permeability, **logBB:** Predicted brain/blood partition coefficient, **PMDCK:** Predicted apparent MDCK cell permeability, **PM:** Number of likely metabolic reactions, **CNSAS:** Predicted central nervous system activity score, **%HOA:** Predicted human oral absorption percent, **VRF:** Number of violations of Lipinski's rule of five. The rules are: MW < 500, logP < 5, DHB ≤ 5, AHB ≤ 10, Positive PSA value. **VRT:** Number of violations of Jorgensen's rule of three. The three rules are: logS > −5.7, PCaco > 22 nm/s, PM < 7.

3.2.2. Enzyme kinetics

The mechanisms of AChE and MAO-B inhibition were investigated by enzyme kinetics. The type of inhibition was estimated by the linear Lineweaver-Burk graphics. The substrate velocity curves in the absence and presence of the most potent compounds (**3g** for AChE and **3h** for MAO-B) were recorded in the enzyme kinetics analysis. These compounds were prepared at concentrations of $IC_{50}/2$, IC_{50} and $2 \times IC_{50}$. The different substrate concentrations ranging from 600 μM to 18.75 μM for AChE and from 20 μM to 0.625 μM for MAO-B were used to gain the initial velocity measurements. The K_i (intercept on the x-axis) values of compounds were determined from the secondary plot of the K_m/V_{max} (slope) versus varying concentrations [34]. The graphical analysis of steady-state inhibition data for AChE and MAO-B enzymes are shown in Figs. 1 and 2, respectively.

The type of inhibition can be determined as mixed-type, competitive, uncompetitive, or noncompetitive by the Lineweaver-Burk plot. In an uncompetitive type inhibition graphic, there are non-diagonal parallel lines. If the lines do not cross x- or y-axis at the same point, it is called as mix type as observed in Fig. 1. Competitive inhibitors have the same intersection point on the y-axis but have different slopes and intersection points on the x-axis between the two sets of data, while noncompetitive inhibitors have plots with the same intersection on x-axis but there are different slopes and intersection on y-axis as observed in Fig. 2. These results show that compounds **3g** and **3h** are mixed-type and non-competitive inhibitors, respectively. Namely, both compounds can bind to the free enzyme or the enzyme-substrate complex. If any type of the above graphics is observed in Lineweaver-Burk plots, this mean that tested compound is a reversible inhibitor, which binds to enzyme by noncovalent interactions as hydrophobic interactions, ionic bonds, and hydrogen bonds without forming any chemical bonds or reactions with the enzyme. These interactions occur quickly and can be easily removed. For this reason, the complex of the enzyme and inhibitor is rapidly degraded just before the irreversible inhibition. Because of the ability to bind reversibly to biomolecules, such inhibitors present a lower risk of side effects than irreversible inhibitors. As a result, enzyme kinetics studies have displayed the biological significance of compounds **3g** and **3h** owing to their mixed-type and noncompetitive inhibition potencies, respectively, as opposed to irreversible enzyme inhibitors.

3.2.3. ADME and BBB permeability predictions

Most of the clinical trials for new drug development are failing due to insufficient ADME (absorption, distribution, metabolism and excretion) properties of the drug candidate compound. Failures that occur during the last phases of these studies lead to an increase in the cost of new drug development. Early identification of problematic issues can significantly reduce the amount of wasted time and funds, and can rationalize the overall development process. Therefore, the pharmacokinetic properties of new drug candidates are one of the important issues that should be assessed as early as possible in the drug development process. ADME estimation can be used to focus on lead optimization to improve the preferred properties of a compound [38]. Hence, predictions of ADME parameters of synthesized compounds (**3a–3p**) were carried out by *QikProp 4.8* software [35], assessing the violations of Lipinski's rule of five [39] and Jorgensen's rule of three [40]. These rules are good indicators of the ADME properties of new drug candidates, and are necessary for the optimization of a biologically active compound. Molecular weight (MW), number of rotatable bonds (RB), dipole moment (DM), molecular volume (MV), number of hydrogen donors (DHB), number of hydrogen acceptors (AHB), polar surface area (PSA), octanol/water partition coefficient (log P), aqueous solubility (log S), apparent Caco-2 cell permeability (PCaco), number of likely primer metabolic reactions (PM), and percent of human oral absorption (%HOA) are given in Table 4 along with the violations of rules of three (VRT) and five (VRF). As seen in Table 4 all compounds (**3a–3p**) are in agreement with both rules by causing no more than one violation.

In particular, drugs targeting the CNS should pass the blood-brain barrier (BBB) first. Although BBB has a protective nature, the non-penetration of molecules into the BBB is an important obstacle for CNS drug candidates and should be addressed early in the drug discovery process. Thus, the task of predicting the BBB permeability of new compounds is of paramount importance [38]. In the present study the BBB permeability of the synthesized compounds (**3a–3p**) was also estimated by *QikProp 4.8* software [35]. Apparent MDCK cell permeability (PMDCK), brain/blood partition coefficient (log BB), and central nervous system activity scores (CNSAS) were calculated for this purpose. MDCK cells are considered to be a good mimic for the blood brain barrier. According to software predictions, the PMDCK values of < 25 and > 500 nm/s are recommended as poor and great for non-active

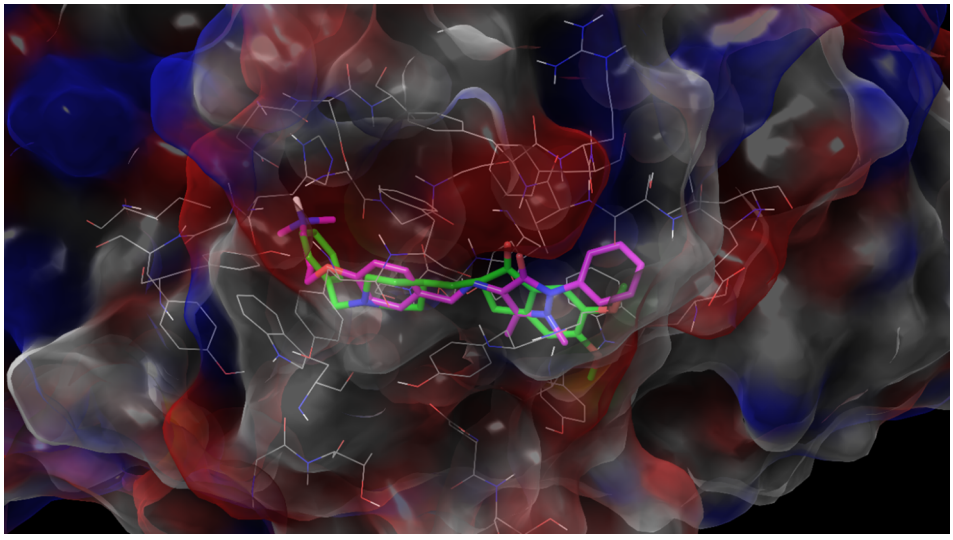

Fig. 3. Three-dimensional pose of compound **3g** (pink colored) and donepezil (green colored) in the enzyme active site (AChE PDB Code: 4EY7).

transport of compound. Besides, in order to pass BBB, logBB and CNSAS have recommended values of −3 to 1.2 and −2 to 2, respectively. It is seen in Table 4 that PMDCK, logBB and CNSAS are in the recommended ranges. Thus, it can be deduced that the synthesized compounds have the ability to pass the BBB, which is extremely important for CNS related drugs.

As a result of the ADME and BBB Permeability estimates, it can be suggested that all synthesized compounds may have a good pharmacokinetic profile.

3.2.4. Molecular docking studies

Docking studies were performed in order to gain more insight into the binding mode of compounds **3g** and **3h** to AChE and MAO-B enzymes. Studies were carried out by using the X-ray crystal structures of *Homo sapiens* AChE (hAChE PDB ID:4EY7) [36] and MAO-B (PDB ID: 2V5Z) [37] obtained from Protein Data Bank server (www.pdb.org).

The docking poses of the compound **3g** are presented in Figs. 3 and 4. According to the superimposition poses of this compound with donepezil, it is clearly understood that **3g** binds to AChE enzyme in a similar position with donepezil due to the dual binding sites. Lipophilic part of the compound is consist of 1,5-dimethyl-2-phenyl-1H-pyrazol-3(2*H*)-one scaffold, while dimethylaminoalkyl side chain constitutes a polar basic center. The docking poses indicate that PAS region of AChE interact with lipophilic group in the structure, whereas the polar and basic groups bind to the CAS region of the enzyme.

It is observed that carbonyl of pyrazole interacts with amino group of Phe295 by forming a hydrogen bond. Another hydrogen bond is related to nitrogen of dimethyamino group. This nitrogen atom forms a hydrogen bond with the carboxyl of Glu202. An efficient binding is also provided by the formation of cation-π interaction between this nitrogen atom and Trp86. The other important factor of binding to the active site is π-π interaction between 1,4-disubstituted phenyl and Tyr337. Docking results also show that extended carbon chain enhances the van der Waals interactions with the amino acids in the active site and intensifies the proper bonding.

Three-dimensional pose of compound **3h** in the active site of MAO-B is presented in the Fig. 5. Interactions between enzyme and inhibitor is displayed in the Fig. 6. The compound **3h** adequately binds to amino acid residues, lining the cavity by overlapping at the same site and, locating very near the FAD cofactor. The docking poses on MAO-B reveal that the carbonyl of pyrazole establishes a hydrogen bond with amino of Cys172. There is a π-π interaction between pyrazole and

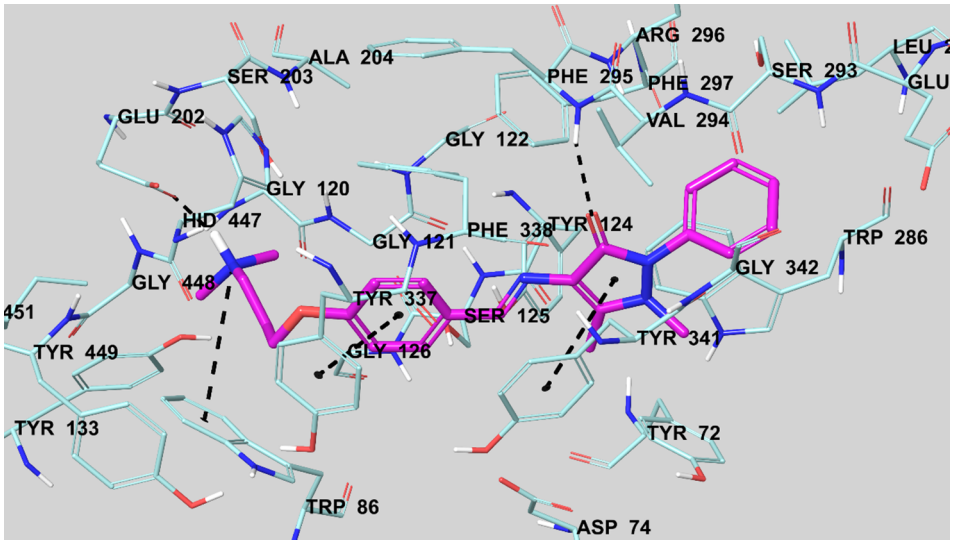

Fig. 4. The interacting mode of compound **3g** in the active region of AChE. The inhibitor, colored with pink, and the important residues, colored with turquoise, in the active site of the enzyme are presented by tube model.

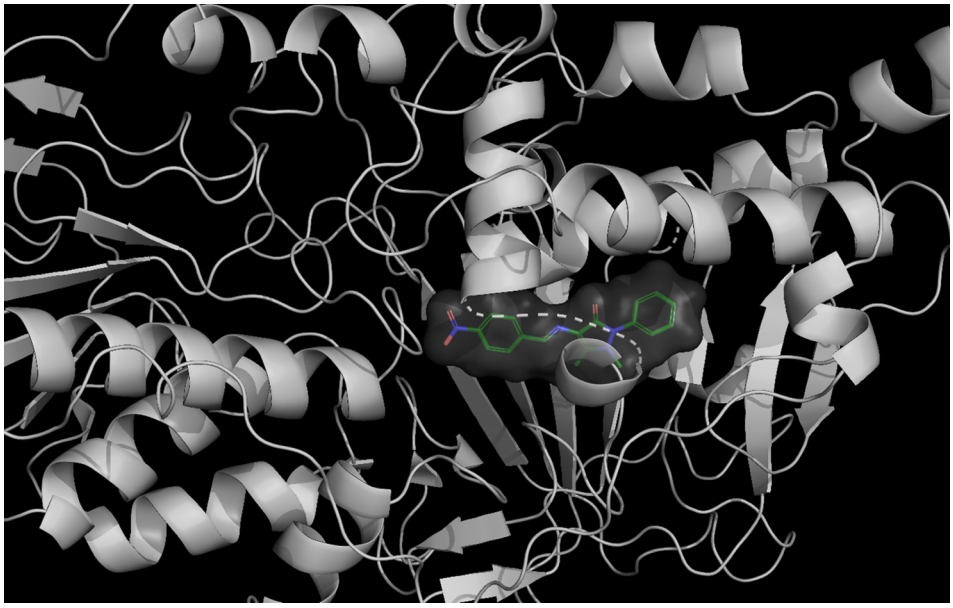

Fig. 5. Three-dimensional pose of compound **3h** in the enzyme active site (MAO-B PDB Code: 2V5Z).

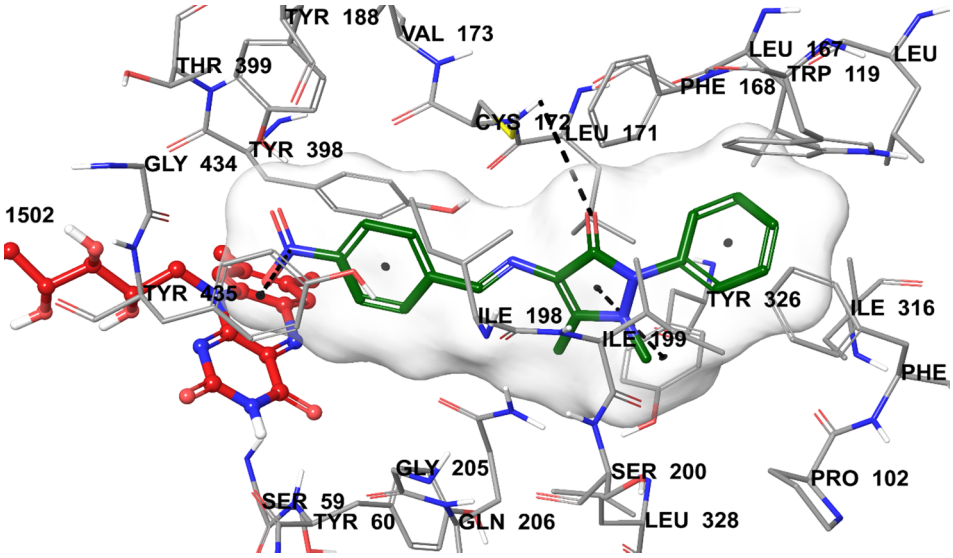

Fig. 6. The interacting mode of compound **3h** in the active region of MAO-B. The inhibitor and the important residues in the active site of the enzyme are presented by tube model. The inhibitor is colored with dark green. The FAD molecule is colored red with ball and stick model.

phenyl of Try32. The nitrogen atom of nitro group forms cation-π interaction with phenyl of Tyr435. It is thought that this interaction is important to explain why compound **3h** is the most active derivative in the series. Thus, it may be suggested that the presence of an electron withdrawing group such as nitro has a positive contribution to the activity.

4. Conclusion

In this study, we synthesized some Schiff bases as cholinesterase and MAO inhibitors. According to activity results, compounds **3g** and **3h** displayed the highest inhibition towards AChE and MAO-B, respectively. In an effort to explain their inhibitory effects, the enzyme kinetic and docking studies were applied. ADME and BBB permeability predictions enhanced the biological significance of these compounds. Consequently, this study presents important results for developing new enzyme inhibitors, which may be beneficial for neurodegenerative diseases such as Parkinson's and Alzheimer's diseases.

Appendix A. Supplementary material

Supplementary data to this article can be found online at https://doi.org/10.1016/j.bioorg.2018.11.016.

References

[1] K.Y. Yeong, M.A. Ali, A.C. Wei, T.S. Choon, K.Y. Khaw, V. Murugaiyah, H. Osman, V.H. Masand, Bioorg. Chem. 49 (2013) 33–39.
[2] C. Eggers, K. Herholz, E. Kalbe, W.D. Heiss, Neurosci. Lett. 408 (2006) 46–50.
[3] B.N. Sağlık, S. Ilgın, Y. Özkay, Eur. J. Med. Chem. 124 (2016) 1026–1040.
[4] M.B. Colovic, D.Z. Krstic, T.D. Lazarevic-Pasti, A.M. Bondzic, V.M. Vasic, Curr. Neuropharmacol. (2013) 11315–11335.
[5] P. Meena, V. Nemaysh, M. Khatri, A. Manral, P.M. Luthra, M. Tiwari, Bioorg. Med.

Chem. 23 (2015) 1135–1148.
[6] B.M. McGleenon, K.B. Dynan, A.P. Passmore, J. Clin. Pharmacol. 48 (1999) 471–480.
[7] M. Mehta, A. Adem, M. Sabbagh, Int. J. Alzheimers Dis. (2012) 1–9.
[8] R.R. Ramsay, Curr. Top. Med. Chem. 12 (2012) 2189–2209.
[9] L. Legoabe, A. Petzer, J.P. Petzer, Drug Des. Devel. Ther. 9 (2015) 3635–3644.
[10] M. Garcia-Miralles, J. Ooi, C.F. Bardile, L.J. Tan, M. George, C.L. Drum, R.Y. Lin, M.R. Hayden, M.A. Pouladi, Exp. Neurol. 278 (2016) 4–10.
[11] H. Checkoway, G.M. Franklin, P. Costa-Mallen, Neurology 50 (1998) 1458–1461.
[12] B. Kaya-Çavuşoğlu, B.N. Sağlık, Y. Özkay, B. İnci, Z.A. Kaplancıklı, Bioorg. Chem. 76 (2018) 177–187.
[13] B. Kaya-Çavuşoğlu, B.N. Sağlık, D. Osmaniye, S. Levent, U. Acar-Çelik, A.B. Karaduman, Y. Özkay, Z.A. Kaplancıklı, Molecules 23 (2018) 60.
[14] A. Ansari, A. Ali, M. Asif, Biologically active pyrazole derivatives, New J. Chem. 41 (2017) 16–41.
[15] K. Karrouchi, S. Radi, Y. Ramli, J. Taoufik, Y.N. Mabkhot, F.A. Al-Aizari, M. Ansar, Molecules 23 (2018) 134.
[16] D. Secci, A. Bolasco, P. Chimenti, S. Carradori, Curr. Med. Chem. 18 (2011) 5114–5144.
[17] A. Rahman, M. Choudhary, Multifunctional Enzyme Inhibition for Neuroprotection-A Focus on MAO, NOS and AChE Inhibitors, Drug Design and Discovery in Alzheimer's Disease, 1st ed., Bentham Science Publishers, 2015, pp. 291–365.
[18] F. Chimenti, A. Bolasco, F. Manna, D. Secci, P. Chimenti, O. Befani, P. Turini, V. Giovanni, B. Mondovi, R. Cirilli, F. La Torre, J. Med. Chem. 47 (2004) 2071–2074.
[19] R. Fioravanti, A. Bolasco, F. Manna, F. Rossi, F. Orallo, M. Yanez, A. Vitali, F. Ortuso, S. Alcaro, Bioorg. Med. Chem. Lett. 20 (2010) 6479–6482.
[20] M. Karuppasamy, M. Mahapatra, S. Yabanoglu, G. Ucar, B.N. Sinha, A. Basu, N. Mishra, A. Sharon, U. Kulandaivelu, V. Jayaprakash, Bioorg. Med. Chem. 18 (2010) 1875–1881.
[21] M. Jagrat, J. Behera, S. Yabanoglu, A. Ercan, G. Ucar, B.N. Sinha, V. Sankaran, A. Basu, V. Jayaprakash, Bioorg. Med. Chem. Lett. 21 (14) (2011) 4296–4300.
[22] N. Mishra, D. Sasmal, Bioorg. Med. Chem. Lett. 21 (7) (2011) 1969–1973.
[23] M.S. Shah, S.U. Khan, S.A. Ejaz, S. Afridi, S.U.F. Rizvi, M. Najam-ul-Haq, J. Iqbal, Biochem. Biophys. Res. Commun. 482 (4) (2017) 615–624.
[24] S. Chigurupati, M. Selvaraj, V. Mani, K.K. Selvarajan, J.I. Mohammad, B. Kaveti, H. Bera, V.R. Palanimuthu, L.K. Teh, M.Z. Salleh, Bioorg. Chem. 67 (2016) 9–17.
[25] S.M. Mehdi, R.M. Ghalib, R. Hashim, M.F.C. Guedes da Silva, O. Sulaiman, V. Murugaiyah, M.M. Marimuthu, M. Naqvi, J. Mol. Struct. 1049 (2013) 488–493.
[26] G. Ucar, N. Gokhan, A. Yesilada, A.A. Bilgin, Neurosci. Lett. 382 (2005) 327–331.
[27] V. Jayaprakash, B.N. Sinha, G. Ucar, A. Ercan, Bioorg. Med. Chem. Lett. 18 (2008) 6362–6368.
[28] A. Kumar, S. Jain, M. Parle, N. Jain, P. Kumar, EXCLI J. 12 (2013) 1030–1042.
[29] A.P. Stankyavichyus, P.B. Terent, O.A. Solov, Chem. Heterocyc. Compd. 9 (1990) 1243–1247.
[30] V.M. Hudlicky Reductions in organic chemistry. Ellis Horwood Limited, Chichester, England (1984) 28-29, 0–85312-345-4.
[31] K.M. Khan, A. Khan, M. Taha, U. Salar, A. Hameed, N.H. Ismail, W. Jamil, S.M. Saad, S. Perveen, S.M. Kashif, J. Chem. Soc. Pak. 37 (4) (2015) 802–811.
[32] G.L. Ellman, K.D. Courtney, V. Jr, R.M. Feather-Stone Andres, Biochem. Pharmacol. 7 (1961) 88.
[33] Ü. Demir Özkay, Ö.D. Can, B.N. Sağlık, U. Acar Çevik, S. Levent, Y. Özkay, S. Ilgın, Ö. Atlı, Bioorg. Med. Chem. Lett. 26 (2016) 5387–5394.
[34] Ö.D. Can, D. Osmaniye, Ü. Demir Özkay, B.N. Sağlık, S. Levent, S. Ilgın, M. Baysal, Y. Özkay, Z.A. Kaplancıklı, Eur. J. Med. Chem. 131 (2017) 92–106.
[35] QikProp, version 4.8, Schrödinger, LLC, New York, NY, USA, 2016.
[36] J. Cheung, M.J. Rudolph, F. Burshteyn, M.S. Cassidy, E.N. Gary, J. Love, C.F. Matthew, J.J. Height, J. Med. Chem. 55 (2012) 10282–10286.
[37] B. Claudia, J. Wang, L. Pisani, C. Caccia, A. Carotti, P. Salvati, D.E. Edmondson, A. Mattevi, A. J. Med. Chem. 50 (2007) 5848–5852.
[38] H.V. De Waterbeemd, E. Gifford, Nat. Rev. Drug Discov. 2 (2013) 192–204.
[39] C.A. Lipinski, F. Lombardo, B.W. Dominy, P.J. Feeney, P.J. Adv, Drug Deliv. Rev. 46 (2001) 3–26.
[40] W.L. Jorgensen, E.M. Duffy, Adv. Drug Deliv. Rev. 54 (2002) 355–366.